Investigation of microstructural features in regenerating bone using micro computed tomography

A. C. JONES, A. SAKELLARIOU, A. LIMAYE, C. H. ARNS, T. J. SENDEN, T. SAWKINS, M. A. KNACKSTEDT
Department of Applied Mathematics, Research School of Physical Sciences and Engineering, Australian National University, ACT 0200, Australia

D. ROHNER
Cranio-Facial-Center (cfc) Hirslanden, CH-5000 Aarau, Switzerland

D. W. HUTMACHER
Division of Bioengineering, Faculty of Engineering, Department of Orthopaedic Surgery, Faculty of Medicine, National University of Singapore, Singapore 119260

A. BRANDWOOD, B. K. MILTHORPE*
Graduate School of Biomedical Engineering, University of New South Wales, Sydney, NSW 2052, Australia
E-mail: b.milthorpe@unsw.edu.au

We illustrate some of the uses of micro-computed tomography (micro-CT) to study tissue-engineered bone using a micro-CT facility for imaging and visualizing biomaterials in three dimensions (3-D). The micro-CT is capable of acquiring 3D X-ray CT images made up of 2000^3 voxels on specimens up to 5 cm in extent with resolutions down to 2 μm. This allows the 3-D structure of tissue-engineered materials to be imaged across orders of magnitude in resolution. This capability is used to examine an explanted, tissue-engineered bone material based on a polycaprolactone scaffold and autologous bone marrow cells. Imaging of the tissue-engineered bone at a scale of 1 cm and resolutions of 10 μm allows one to visualize the complex ingrowth of bone into the polymer scaffold. From a theoretical viewpoint the voxel data may also be used to calculate expected mechanical properties of the tissue-engineered implant. These observations illustrate the benefits of tomography over traditional techniques for the characterization of bone morphology and interconnectivity. As the method is nondestructive it can perform a complimentary role to current histomorphometric techniques.

Introduction

Traditional histological techniques of evaluating the mineralization and neovascularization within polymer scaffolds for bone replacement are based on two-dimensional (2-D) histological sections. Usually only one or two sections are taken from a relatively large piece of implant. Much important information is lost in this process relating to the distribution of mineralizing tissue, the proportion in any one area of the scaffold, any long-term organization of the mineralizing tissue and the relationship of the mineralizing tissue to the host tissue.

Micro-computed tomography (micro-CT) is a non-destructive technique that can be used to image specimens at the micron scale in 3-D. Ritman *et al.* [1–5] have investigated bone deposition rates in several tissues using micro-CT, while other groups have investigated the effects of osteoarthritic disease upon bone structure [6–11]. Ruegsegger and Muller have quantitatively investigated cancellous bone [12–18].

This work describes progress made towards the identification and quantification of microstructural features of mineralizing tissue within a polycaprolactone (PCL) scaffold implanted into the orbital wall of a pig.

Materials and methods

Sample preparation

Tissue engineered scaffolds were prepared by fused deposition modeling as reported elsewhere [19–21]. Under anesthesia, surgical defects of approximately $1\,cm^2$ were created in the orbital wall of mature pigs and reconstructed using PCL scaffolds infused with

*Author to whom all correspondence should be addressed.

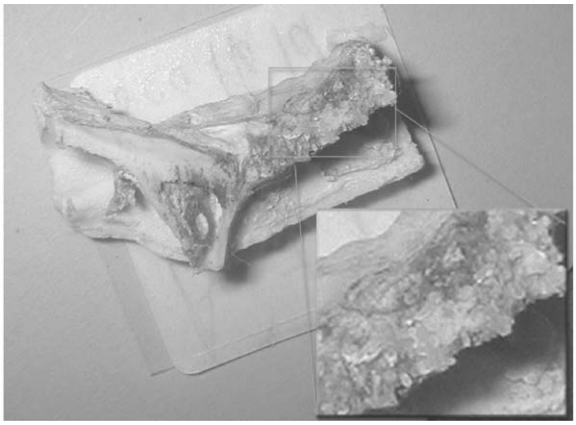

Figure 1 Explanted, fixed and dried sample of marrow-inoculated PCL scaffold from orbital bone (porcine model).

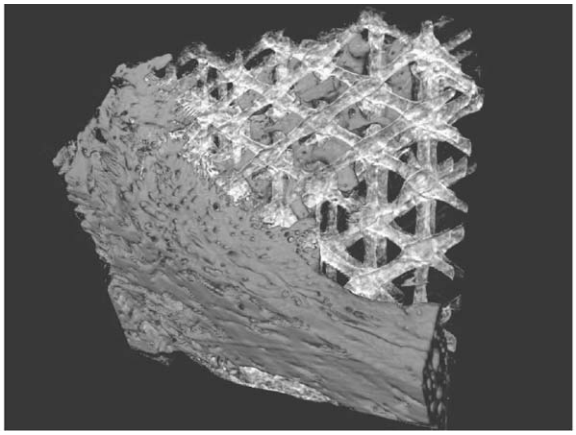

Figure 2 Rendered 3-D tomographic data of mineralizing scaffold and original bone. Scaffold shows as semitransparent, white material, while calcified areas (old, bottom left, and new, top right, bone are shown as darker colour).

autologous bone marrow taken at the time of implantation. The scaffold was explanted at three months, fixed in buffered formalin, defatted, and dried [19]. Fig. 1 shows the sample as received for micro-CT imaging.

The micro-CT apparatus was developed and built at the Department of Applied Mathematics, Australian National University [22] and has a cone beam geometry, thus allowing the magnification to be set by adjusting the ratio of the distance between the X-ray source and the specimen to the distance between the X-ray source and the camera. The limiting resolution is between 2 and 5 μm, depending on operating voltage (30–120 kV). The camera is capable of acquiring X-ray images of 2048 × 2048 pixels with a depth of 16 bits per pixel. High-contrast and low-noise images of the internal structure within biomaterials can be generated due to the large range of X-ray energies available from the source and the large dynamic range of the X-ray camera.

Tomographic data, corrected for optical and camera distortion, were acquired of the specimen (80 kV, 10 × magnification, 10 s exposure, 1800 projections) and reconstructed by locally written software using standard algorithms (Feldkamp technique [23]). To process data, an AlphaServer SuperComputer (see: http://nf.apac.edu.au/facilities/sc/hardware.php) is used and takes 128 CPUs approximately 4 h to generate a 2048^3 voxel tomogram.

The tissue-engineered bone was first imaged at a magnification factor of × 7.14, resulting in a voxel size of 9.4 μm. A 2-mm thick bone filter on the X-ray source was used for this specimen. The entire acquisition took approximately 16 h with an exposure time of 32 s/projection.

A set of representative slices from the reconstructed tomographic data was first developed. These 2-D slices were used to generate intensity histograms for various regions: 6100 (pore/soft tissue), 7800 (polymer) and 12 800 (mineralized tissue). To differentiate the image into the three separate phases two-phase separation steps were performed; between the pore and solid phases (cut-off thresholds 6800 : 7250), and between the polymer and mineralized bone phases (10 000 : 12 000). Indicator kriging [25] is then performed to define the phases.

After phase separation, 3-D visualizations of the distribution of polymer and mineralized phase within the specimen were generated (Fig. 2).

Higher resolution imaging and mechanical property calculation

A number of features could not be visualized within the bone at the resolution described above; this led to a study of subsets of the original system at higher resolutions. In particular, the region of bone ingrowth into the scaffold was examined at higher resolution. From the higher resolution images, voxel data were then used to assign mechanical properties (bone or pore) to each voxel. Overall elastic modulus was then calculated by the two-phase finite element method of Arns *et al*. [22]. Bone voxels were assumed to have equivalent properties to cortical bone ($K_{\text{bone}} = 17\,\text{GPa}, G_{\text{bone}} = 6.3\,\text{GPa}$) and the pores were assumed to be either air or water.

Results and discussion

It was possible to resolve the original polymer scaffold and regions of densely mineralized tissue using phase identification techniques from the reconstructed tomograms. However, large regions of the scaffold exhibited no or very weak mineralization.

Three phases are evident in the image of Fig. 2; strongly mineralized (dark red), polymer (white) and poorly mineralized/pore phase (dark). The host bone is shown in the lower right corner. The PCL scaffold exhibits regular lattice shaped struts. There are a number of interesting features visible including the effects of shaping at implantation on distortion and cracking of the scaffold. Three dimensional imaging at this resolution allows the study of the morphology and surface properties of the scaffold matrix. The large region of strongly mineralized phase within the scaffold is ascribed to new bone formation, but this phase lies away from the host bone in the sample provided. Little to no bone ingrowth into the scaffold from the original host bone is noted. The only growth visible is as minute ''fingers'' on the border of the scaffold. It is unclear from these images whether the bone within the scaffold is connected to the host bone. It is unclear from these data whether the observed mineralizing tissue ingrowth is from the host, or as a result of the marrow aspirate cells.

The architecture of the bone is defined by the scaffold giving the new bone a regular lattice structure. Small

porous regions are observed within the newly mineralized bone, these are presumably associated with incomplete bone growth and the presence of a neovascular network. The new bone ingrowth follows a strongly preferred orientation along the plane of fabrication of the original scaffold (generated using a 0/60/120 degree pattern in the FDM process [24]). It was also observed that the new bone ingrowth is primarily isolated to a single slice within the scaffold, on average $\sim$ 400-μm thick perpendicular to the fabrication plane, while growth within the plane of fabrication extends around 3 mm in one direction and about 1.4 mm in the other. This preference for orientation would not appear to be due to vascular accessibility as pore sizes are comparable along all three directions within the scaffold.

Three dimensional imaging allows one to investigate the potential connectivity between the host bone and the bone ingrowth within the scaffold. High resolution imaging of the region of bone ingrowth close to the host bone reveals that the new bone is disconnected from the host bone. It was noted that the bone ingrowth comes very close to the host bone, but has a distinct interface with no direct connection. This observation, along with the minute amount of bone growth seen advancing from the host bone, would indicate that there is no significant revascularization progressing from the intact surface of the host bone.

A downloadable version of the 3-D movie of the sample is available at: http://wwwrsphysse.anu.edu.au/appmaths/ct_movies/ which makes visualization of the described features much more noticeable than static 2-D figures.

The very high resolution imaging of the newly forming bone also displays some interesting features. A number of micropores are visible within the highly mineralized tissue. The pores are not highly connected and display a disorderly architecture (Fig. 3). This may be simply due to differences in the mineral content, as the thresholding process will produce ''pores'' if the X-ray absorbance of a set of voxels decreases below the threshold level. Alternatively, active regions of cellular expansion, prior to mineralization, may produce a similar result as may the formation of a neovascular network.

Figure 3 Rendered 3-D tomographic data of mineralized new bone, viewed with transparent surfaces. Porous microstructure is evident within the regenerating tissue.

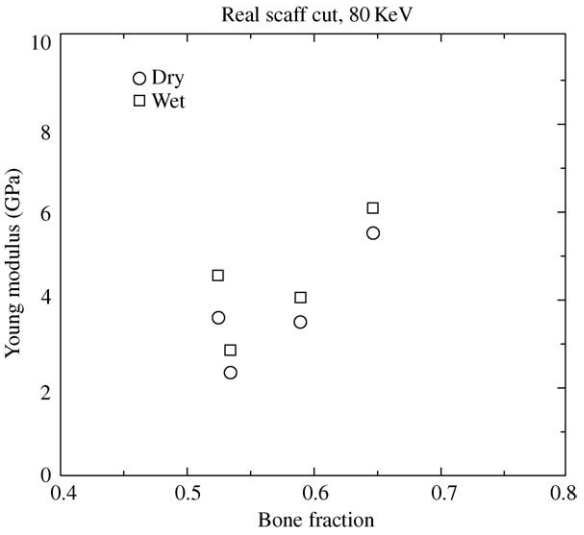

Figure 4 Predicted linear elastic properties for 1.6 mm^3 subvolumes of regenerated bone tissue. Pore voxels were given elastic properties of air (dry) and water (wet) for different simulations.

Finite element modeling [22] was performed on 160^3 voxel (1.6 mm^3) subvolumes of the regenerated bone. Voxels were assigned elastic properties based on a two-phase model ($K_{bone} = 17\,GPa, G_{bone} = 6.3\,GPa$). The predicted Young's modulus for the new tissue (Fig. 4) was comparable to human bone of the same porosity [19].

Further work is planned to visualize and quantify the possible microvascular network and to correlate X-ray density with mechanical properties using nano-identation.

Conclusion

Micro-computed tomography has provided much useful information in recent years about bone and tissue growth and structure. As micro-CT instruments increase in resolution and computing resources become available, more higher detailed information becomes available. The 3-D nature of this information means that much improved visualization of relationships is now possible. This paper has used micro-CT at its highest resolution to demonstrate the usefulness of this technique in visualizing the mineralization of tissue-engineered bone constructs. The observations regarding the lack of host bone outgrowth, the directionality of new bone formation in a structured scaffold and the possibility of visualizing microvasculature in newly forming bone, all point to the potential for this technique to provide valuable information about the processes involved in tissue engineering new bone.

Acknowledgments

We would like to thank all the people involved in the development of the porcine model and the micro computed tomography equipment and the visualization programming (Holger Averdunk, Adrian P. Sheppard and Rob Sok).

This project was supported in part by grants from the Australian Research Council (ARC A10007257, A10007207, DP0345886), and the National University

of Singapore (NUS Young Investigator Grant WBS 397 000 003 650).

We would also like to thank the Australian Partnership for Advanced Computing for providing substantial time on the supercomputer network.

References

1. M. D. BENTLEY, M. C. ORTIZ, E. L. RITMAN and C. ROMERO, *Am. J. Physiol. – Regul. Integr. C.* **282** (2002) 1267.
2. E. L. RITMAN, *J. Cell. Biochem.* **39** (2002) 116.
3. L. A. FITZPATRICK, R. T. TURNER and E. R. RITMAN, *Endocrinology* **144** (2003) 2214.
4. C. C. KO, W. H. DOUGLAS, R. DELONG, M. D. ROHRER, J. Q. SWIFT, J. S. HODGES, K. N. AN and E. L. RITMAN, *J. Dent. Res.* **82** (2003) 585.
5. E. A. MARTIN, E. L. RITMAN and R. T. TURNER, *Bone* **32** (2003) 261.
6. D. K. DEDRICK, S. A. GOLDSTEIN, K. D. BRANDT, B. L. O'CONNOR, R. W. GOULET and M. ALBRECHT, *Arthritis Rheum.* **36** (1993) 1460.
7. J. H. KINNEY, J. T. RYABY, D. L. HAUPT and N. E. LANE, *Technol. Health Care* **6** (1998) 349.
8. C. A. LILL, A. K. FLUEGEL and E. SCHNEIDER, *Osteoporos. Int.* **13** (2002) 480.
9. S. NISHIDA, H. TSURUKAMI, A. SAKAI, T. SAKATA, S. IKEDA, M. TANAKA, M. ITO and T. NAKAMURA, *Bone* **30** (2002) 872.
10. C. A. LILL, U. V. GERLACH, C. ECKHARDT, J. GOLDHAHN and E. SCHNEIDER, *Osteoporos. Int.* **13** (2002) 407.
11. F. MCLAUGHLIN, J. MACKINTOSH, B. P. HAYES, A. MCLAREN, I. J. UINGS, P. SALMON, J. HUMPHREYS, E. MELDRUM and S. N. FARROW, *Bone* **30** (2002) 924.
12. R. MULLER, *Phys. Med. Biol.* **39** (1994) 145.
13. R. MULLER, M. HAHN, M. VOGEL, G. DELLING and P. RUEGSEGGER, *Bone* (1996) 215.
14. R. MULLER, T. HILDEBRAND, H. J. HAUSELMANN and P. RUEGSEGGER, *Technol. Health Care* **4** (1996) 113.
15. T. HILDEBRAND, A. LAIB, R. MULLER, J. DEQUEKER and P. RUEGSEGGER, *J. Bone Miner. Res.* **14** (1999) 1167.
16. R. MULLER, H. VAN CAMPENHOUT, B. VAN DAMME, G. VAN DER PERRE, J. DEQUEKER, T. HILDEBRAND and P. RUEGSEGGER, *Bone* **23** (1998) 59.
17. P. RUEGSEGGER, in ''Bone Mechanics Handbook'', edited by S. C. Corwin (CRC Press, Boca Raton, 2001) chapter 9, p. 1.
18. P. RUEGSEGGER, B. KOLLER and R. MULLER, *Calcif. Tissue Int.* **58** (1996) 24.
19. D. W. HUTMACHER, D. ROHNER, P. SEE, K. C. TAN, V. YEOW, S. T. LEE, A. BRENTWOOD and T. SCHANTZ, in ''Polymer Based Systems in Tissue Engineering, Replacement and Regeneration'' (Kluwer Academic Publishers, The Netherlands, 2002) p. 333.
20. D. W. HUTMACHER, *Biomaterials* **21** (2000) 2529.
21. D. W. HUTMACHER, *J. Biomater. Sci. Polym. Ed.* **12** (2001) 107.
22. C. H. ARNS, M. A. KNACKSTEDT, W. V. PINCZEWSKI and E. J. GARBOCZI, *Geophysics* **67** (2002) 1396.
23. L. A. FELDKAMP, *J. Optic. Soc. Am. A* **1** (1984) 612.
24. I. ZEIN, D. W. HUTMACHER, K. C. TAN and S. H. TEOH, *Biomaterials* **23** (2002) 1169.
25. W. OH and W. B. LINDQUIST, *IEEE Trans. Pattern Anal. Mach. Intel.* **21** (1999) 590.

Received 4 October
and accepted 10 October 2003